applied sciences

MDPI

Article

An Investigation on the Synthesis of Alkali Activated Materials from Thermally Modified Clays

Guilherme Ascensão [1,*], Enrico Bernardo [2] and Victor M. Ferreira [1]

[1] RISCO, Department of Civil Engineering, University of Aveiro, 3810-193 Aveiro, Portugal
[2] Department of Industrial Engineering, University of Padova, 35131 Padova, Italy
* Correspondence: guilhermeascensao@ua.pt; Tel.: +351-966944248

Abstract: The sustainability and economic competitiveness of alkali activation technology greatly depends on expanding the raw materials database with locally available resources. Therefore, a notable trend has been witnessed toward the exploitation of common clays as alternatives to well-established solid aluminosilicate precursors due to their availability and wide geographical distribution. However, common clays are complex and dedicated research is needed to tailor synthesis procedures and mix designs for different clay resources. This paper describes the outcomes of a study conducted to investigate the influence of several synthesis parameters (solid-to-liquid ratio, NaOH molarity, Si availability, and curing conditions) on the properties of alkali activated binders produced from different thermally modified clays. Optimal synthesis conditions for benchmark metakaolin systems have been identified and binders were produced with progressive dosages of metakaolin replacement by common local clays. Fundamental physical and mechanical properties such as apparent density, open porosity, water absorption, and compressive strength were examined at different curing ages, and X-ray diffraction (XRD) was used to provide complementary mineralogical insights. By combining the effects of the parameters studied, mortar specimens were produced with the developed binders, reaching compressive strength values exceeding 28.2 ± 0.1 MPa, a bulk density as low as 1.78 ± 0.0 g/cm^3, and open porosity and water absorption values lower than 15% and 8%, respectively. These properties are comparable to those of conventional hydraulic products, which presents them as interesting candidates for construction. Ultimately, this work aims to contribute with valuable insights toward the valorization of a large group of unexploited clay precursors by demonstrating the feasibility of producing technologically competitive alkali activated materials with little or no use of the prime precursors, thus adding to the extant knowledge and contributing to future scientific and industrial developments in this field.

Keywords: alternative binders; alkali activated materials; secondary resources; valorization of common clays

Citation: Ascensão, G.; Bernardo, E.; Ferreira, V.M. An Investigation on the Synthesis of Alkali Activated Materials from Thermally Modified Clays. *Appl. Sci.* **2022**, *12*, 9085. https://doi.org/10.3390/app12189085

Academic Editor: Asterios Bakolas

Received: 19 August 2022
Accepted: 5 September 2022
Published: 9 September 2022

1. Introduction

In the coming decades, global tensions and conflicts over natural resources, social inequality, forced migration, and global economic instability will be exacerbated by rampant climate changes if profound actions are not immediately taken to modify our current development models. Global warming is among the most pressing environmental problems that should be prioritized when tackling climate change, and anthropologic greenhouse gas (GHG) emissions must be drastically reduced. GHGs are mostly driven by CO_2 emissions, which account for approximately 80% of the total GHG [1]. Carbon capture and storage technologies are expected to deliver massive CO_2 uptakes [2,3], but these technologies still require massive capital investments and elevated operating costs that throttle their economic feasibility and prevent their worldwide spread with meaningful global impacts. Therefore, redefining our current industrial and manufacturing technologies has

become urgent to reduce GHG emissions, limit the rate of climate change progression, and meet the UN Sustainable Development Goals. The importance of the built environment in this matter can be gleaned from the numbers: the construction and operation of buildings consumes approximately 36% of all energy produced worldwide, and accounts for about 39% of global CO_2 emissions [4]. The world's growing population will drive further urbanization needs and concomitant increases in the consumption of building materials. Steel and cement are the most significant building materials and their manufacturing jointly accounts for 12–15% of the global annual CO_2 emissions [5]. Cement production alone represents 20% of industrial CO_2 emissions [2] and global consumption patterns forecast a significant soar in cement demand until 2050 [6]. Therefore, the development of low carbon binders able of replace ordinary Portland cement (OPC) is crucial to address the growing housing needs and decouple social development and well-being from climate change. Emergent binders with environmentally favorable profiles that are being intensely investigated include, among others, belite-rich Portland and belite ye'elimite-ferrite cements [7–11], magnesium-based cements [7], carbonation-hardening cements [7,12], calcined clay limestone cements [13–16], geopolymers, and alkali-activated materials [17–19].

Alkali-activated materials (AAMs) are one of most promising candidates to replace OPC-based products. Initial research on AAMs have been driven by the economic benefits delivered by using industrial by-products as alternative feedstock raw materials, but AAMs have proven to offer excellent technical and environmental performances if some conditions and predicates are safeguarded in the mixture design stage (i.e., thoughtful definition of precursors and alkaline solutions) [17,19–24]. AAMs have also shown enhanced resistance to chemical attack and harsh environments, which can reduce the maintenance costs and recurrent environmental impacts, further increasing the body of arguments supporting AAMs as alternative green binders suitable for the construction sector. In addition, as AAMs are the product of the reaction between an alkali metal source and amorphous or semi-vitreous aluminosilicate precursors, virtually any powdered material with sufficient alumina and silica in a reactive form—meaning sufficiently soluble in alkaline environments—can be used as a precursor, if adequate synthesis conditions are provided. This allows for resilient industrial manufacturing processes and extreme design versatility that allows for the use of locally available resources to address the specific needs and opportunities of regional markets while by-passing the external constraints of global value chains.

Natural and artificial pozzolans (e.g., volcanic ashes [25], pumice [26], and metakaolin [27]) and industrial by-products such as waste glass [28], bauxite residues [29,30], non-ferrous metallurgical slags [17,31,32], and coal and biomass fly ashes [33–36] have been examined as potential precursors, while silicates, hydroxides, carbonates, sulfates, and mixtures thereof can be used as activators. Metakaolin is the most well-established and technologically mature precursor used for AAM production. Metakaolin has attracted attention as a precursor due to its purity and consistent composition as well as its outstanding mechanical properties and the thermal stability of metakaolin-based binders. Technical challenges include the high specific surface area of metakaolin, which often results in poor workability and demand for high water dosages that later result in considerable shrinkage and cracking [37]. Several shrinkage mitigation strategies have been recently described (e.g., heat curing, shrinkage reducing admixtures) and can be used to counteract such deleterious phenomena [32,38].

However, the commercial exploitation of metakaolin-based AAMs can be limited by local shortages and the excessive cost of high-grade kaolinitic clays. The sustainability profiles and green credentials of building materials will be compromised if long transport distances are considered, and the use of endogenous materials as precursors should be favored to further future-proof alkali activation as a scalable, environmentally friendly, and cost-competitive technology. In this view, the interest in using low- and medium-grade clays (kaolinitic and otherwise) abundant in many locations around the globe as metakaolin surrogates is increasing [39–43].

Portugal has plenteous clay resources including kaolinitic clays. Kaolin deposits are distributed mostly in Portugal's northwest region comprising the Lusitanian Meso-Cenozoic basin and a narrow northwest strip located between Viana do Castelo and Aveiro districts [44]. In 2016, Portugal ranked 12th in kaolin production in Europe [45], and although abundant, most kaolin resources are consumed by the local ceramic industry and other high-end markets such as paper, paint, rubber, and agrochemical production. Therefore, highly pure kaolinic clays (i.e., without significant levels of "industrial contaminants" such as quartz, mica, montmorillonite, iron, and titanium oxides) are highly disputed resources that are unlikely to be available for the construction market. Affordable alternatives for AAM manufacturing are needed, and several common clays might have the potential to be used in (partial) lieu of metakaolin. Many of these clays contain kaolinite minerals, but not in the desired quantities for metakaolin commercialization. High iron contents can also be allowed in AAM production and will not constitute a limiting factor as previously demonstrated [17,46,47]. Common clays are considerably cheaper, are available in significant volumes in Portugal, and are even often discharged as industrial waste in activities such as dredging, sand-washing, and kaolin extraction. Therefore, this research focused on the use of a common clay found in central Portugal as precursors, taken as a representative case study of a broad group of currently underutilized clay resources that could potentially be valorized via alkali activation. The influence of various synthesis factors on the fundamental properties of metakaolin systems was examined and taken as the baseline to describe the effects of replacing metakaolin by calcined common clays. Mortar specimens were also produced with progressive contents of common clay to investigate the key fresh and hardened-state properties.

The aim of this groundwork research was to establish the first principles of design for this novel valorization pathway and contribute to the development of innovative building materials that minimize the environmental impacts of construction while enforcing upcycling practices and sustainable development models in Portugal and elsewhere.

2. Experimental Conditions

2.1. Materials

A commercial metakaolin (hereafter MK) was purchased under the name of Argical™ from AGS-mineraux®, Clérac, France. According to the producer, MK is mostly amorphous and almost exclusively composed of SiO_2 and Al_2O_3 at 55.0 and 40.0 wt.%, respectively. A common local red clay (hereafter RC) was provided by a local supplier, Mota Ceramic Solutions®, Oiã, Portugal. RC was calcinated in a laboratory oven at 800 °C with an isothermal step of 2 h (heating rate of 3 °C/min up to 500 °C, and 10 °C/min up to 800 °C) followed by natural cooling. Similar thermal activation procedures have been adopted elsewhere [40,43]. The calcined clay (hereafter CRC) was used to gradually replace MK in the alkali activated binders and mortars (the mix proportions are further detailed in Section 2.2). Densified silica fume (hereafter SF; Elkem Microsilica® Grade 940, ELKEM, Norway) was used as a secondary source of reactive SiO_2. SF has been characterized in previous works and determined to be composed of 95.0 wt.% SiO_2 with minor elements such as CaO, Fe_2O_3, and Al_2O_3 being considered negligible (<0.5 wt.%). The BET specific surface area was determined to be approximately 22,200 m^2/kg [17,48].

Activating solutions were prepared by mixing sodium hydroxide and sodium silicate solutions. Sodium hydroxide solutions (8, 10 and 12 M) were prepared in the laboratory by dissolving sodium hydroxide beads (M = 40.00 g/mol, 97% pure NaOH pellets, CAS [1310-73-2], Scharlab, Sentmenat, Spain) in distilled water. A commercial sodium silicate solution (CAS [338443-3L], 10.6 wt.% Na_2O, 26.5 wt.% SiO_2, and 62.9 wt.% H_2O, Sigma Aldrich, Burlington, EUA) was employed without further elaboration. River sand (≤2 mm) was used as the fine aggregate to prepare the mortar formulations.

2.2. Binder and Mortar Preparation

MK was used as the benchmark precursor to first examine the influence of several compositional factors and establish adequate synthesis conditions for the baseline system. To evaluate the feasibility of using CRC as an alternative precursor and identify optimal MK replacement dosages, different binder compositions were produced with CRC steps of 25.0% up to total MK substitution. The details of the mixture proportions and synthesis factors examined are presented in Table 1. All binder formulations were designed to respect the following molar ratios: (i) $SiO_2/(Al_2O_3 + Fe_2O_3)$ = [3.75–5.15]; (ii) $(Na_2O + K_2O)/(Al_2O_3 + Fe_2O_3)$ = [1.00–1.30]; (iii) $(Na_2O + K_2O)/SiO_2$ = [0.20–0.30]; and (iv) $H_2O/(Na_2O + K_2O)$ = [10.0–15.0] and $SiO_2/(Na_2O + K_2O)$ = [0.50–0.80] in the solution; calculated assuming the precursors complete dissolution and participation in the polymerization reactions. The binder specimens were produced following the procedure described elsewhere by Ascensão et al. [17,29]. In short, it involved: (a) homogenization of sodium silicate and sodium hydroxide solutions at 60 rpm for 300 s; (b) manually mixing the powdered precursors in a plastic container; and (c) mixing the binders' solid components and the alkaline solutions at 60 rpm for 600 s in a mortar mixer. Then, the resulting slurries were transferred to plastic molds (Ø ≈ 20 mm; height ≈ 40 mm), placed inside sealed plastic containers, and left to cure in the mold for 24 h according to the conditions described in Table 2. Alkali activated mortars were prepared following the same procedure but with two additional mixing steps: (i) 30 s mixing step at 60 rpm for introduce the aggregates; and (ii) 60 s mixing step at 95 rpm to further guarantee a proper homogenization. Mortar specimens (4 × 4 × 16 cm^3) were produced with a binder-to-aggregate ratio of 1.0 and cast as prescribed by EN 1015-11 [49]. Mortars were coded after their parent binder using M to mark the difference between them (e.g., R50 represents a binder produced as per Table 1, while MR50 will be used to refer to mortar specimens produced with R50 binders).

Table 1. Experimental plan: Binders' mix design and variables assessed.

	Mixture Proportion (wt.%)					**S/L ***	**C/S ***	**SH/SS ***	**NaOH**	**Curing**	**Factor**
	MK	**SF**	**CRC**	**NaOH**	**Na_2SiO_3**	**wt.%**	**wt.%**	**wt.%**	**mol/dm^3**	**Cond.**	
SL0.90	37.8	9.5	0.0	31.7	21.1	**0.9**	4.0	1.50	10.0	C1	S/L ratio
SL1.00	40.0	10.0	0.0	30.0	20.0	**1.0**	4.0	1.50	10.0	C1	
SL1.10	42.0	10.5	0.0	28.5	19.0	**1.1**	4.0	1.50	10.0	C1	
CS4.00	40.0	10.0	0.0	30.0	20.0	1.0	**4.0**	1.50	10.0	C1	C/S ratio
CS3.50	38.9	11.1	0.0	30.0	20.0	1.0	**3.5**	1.50	10.0	C1	
CS3.00	37.5	12.5	0.0	30.0	20.0	1.0	**3.0**	1.50	10.0	C1	
HS1.50	40.0	10.0	0.0	30.0	20.0	1.0	4.0	**1.50**	10.0	C1	SH/SS ratio
HS1.25	40.0	10.0	0.0	27.8	22.2	1.0	4.0	**1.25**	10.0	C1	
HS1.00	40.0	10.0	0.0	25.0	25.0	1.0	4.0	**1.00**	10.0	C1	
M8	40.0	10.0	0.0	30.0	20.0	1.0	4.0	1.50	**8.0**	C1	NaOH M
M10	40.0	10.0	0.0	30.0	20.0	1.0	4.0	1.50	**10.0**	C1	
M12	40.0	10.0	0.0	30.0	20.0	1.0	4.0	1.50	**12.0**	C1	
C1	40.0	10.0	0.0	30.0	20.0	1.0	4.0	1.50	10.0	**C1**	Curing cond.
C2	40.0	10.0	0.0	30.0	20.0	1.0	4.0	1.50	10.0	**C2**	
C3	40.0	10.0	0.0	30.0	20.0	1.0	4.0	1.50	10.0	**C3**	
R0	37.5	12.5	**0.0**	25.0	25.0	1.0	3.0	1.00	12.0	C3	CRC dosage
R25	28.1	12.5	**9.4**	25.0	25.0	1.0	3.0	1.00	12.0	C3	
R50	18.8	12.5	**18.8**	25.0	25.0	1.0	3.0	1.00	12.0	C3	
R75	9.4	12.5	**28.1**	25.0	25.0	1.0	3.0	1.00	12.0	C3	
R100	0.0	12.5	**37.5**	25.0	25.0	1.0	3.0	1.00	12.0	C3	

* Mass ratios are abbreviated as: S/L—solid to liquid ratio; C/S—calcined clay (MK, CRC, or MK + CRC) to silica fume ratio; SH/SS—sodium hydroxide to sodium silicate ratio.

Table 2. The examined curing conditions.

C1	40 °C ± 95 RH	20 °C ± 95% RH		20 °C ± 65 RH
	1 day	**6 days**		**21 days**
C2	20 °C ± 95 RH	40 °C ± 95 RH	20 °C ± 95 RH	20 °C ± 65 RH
	1 day	**1 day**	**5 days**	**21 days**
C3	20 °C ± 95 RH	40 °C ± 95 RH	20 °C ± 95 RH	20 °C ± 65 RH
	1 day	**5 days**	**1 day**	**21 days**

Time (days)

2.3. Characterization Methods

The precursors' particle size distribution was determined by laser diffraction (Coulter LS230 analyzer) combining the laser diffraction technique and polarization intensity differential scattering (PIDS). The chemical composition of the precursors was obtained using X-ray fluorescence (Philips X'Pert PRO MPD spectrometer), with loss on ignition (LOI) at 1000 °C also determined. The crystallinity of the starting precursors and binders was assessed by X-ray diffraction (XRD). Experiments were carried out on a Bruker D8 Advance (Bruker AXS, Karlsruhe, Germany) (CuKa radiation, 5–70°, 0.05° step, and 1 s/step, with the support of a position sensitive detector) and on a Rigaku Geigerflex D/max-Series instrument (Rgaku Corporation, Tokyo, Japan) (CuKa radiation, 10–80°, 0.02° step and 10 s/step). The phase identification was performed by means of the Match! program package (Crystal Impact GbR, Bonn, Germany), supported by the database ICDD-PDF-2. Binder samples were collected from the mechanical tests after 28 day of curing, ground, sieved (≤63 μm), and kept sealed prior to testing. The bulk density of the binders and mortars was determined by the relation between the weight and volume of each sample. The weight (0.1 g accuracy) and dimensions (0.01 mm accuracy) of each individual specimen were measured after 7 and 28 days of curing. The Archimedes method (using water as the immersion fluid) was employed to evaluate the water absorption and open porosity after 28 days of curing. The compressive strength of the binders was determined using a Universal Testing Machine (Shimadzu model AG-25 TA) running at a displacement rate of 0.5 mm min^{-1}. A minimum of four cylindrical specimens were tested per formulation and curing age (7 and 28 days), and the average strength values are reported here after computing the correction factors for cylindrical specimens as prescribed by ASTM C42/C42M [50]. The compressive strength of the mortar specimens was determined as per EN 1015-11 [49]. To further complement the characterization of the CRC mortars, consistence (flow table test), fresh density, dynamic elasticity modulus, and capillary index were determined as per EN1015-3 [51], EN 1015-6 [52], EN 12504-4 [53], and EN 1015-18 [54], respectively.

3. Results and Discussion

3.1. Precursor Characterization

Figure 1a reports the diffraction analysis of the local common clay, before and after calcination at 800 °C. Considering the intensity of the characteristic diffraction maxima, the content of quartz (PDF#87-0743) appears to be substantial. Accessory mineral phases consisted of feldspar (microcline, PDF#77-0135) and mica (muscovite, PDF#80-0743). Signals consistent with clay minerals such as kaolinite ($Al_2Si_2O_5(OH)_4$, PDF#89-6538) were visible only in the as-received clays, in good agreement with dehydroxylation and transformation into amorphous metakaolin upon calcination. The formation of metakaolin provided initial evidence in favor of the CRC potential as an alternative precursor in alkali activated systems. The enhanced peak at 2θ~23° is consistent with the formation of anhydrous aluminum silicate ($Al_{0.5}Si_{0.75}O_{2.25}$, PDF#37-1480), likely formed by the same dehydroxylation process. Increases in the intensity of the quartz-related peaks are most likely

attributed to the 'concentration' mechanisms, as hydrated minerals undergo obvious mass reductions with dehydroxylation. Thermal decomposition probably did not solely involve clay minerals, but also (partially) muscovite. Similar observations were made by Merabtene et al. [55], who examined the decomposition of muscovite and reported the formation of additional quartz and leucite. The formation of leucite cannot be proved here considering the overlap with signals from microcline.

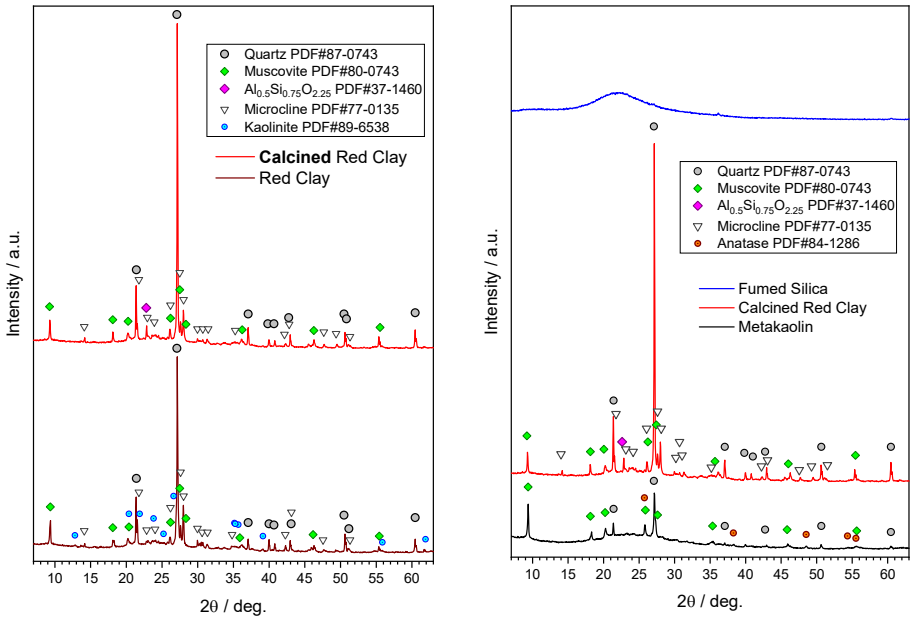

(**a**) (**b**)

Figure 1. Diffraction analysis of the starting raw materials used to synthesize AAM binders: (**a**) comparison between the local red clay before and after calcination; (**b**) comparison between the commercial metakaolin (MK), local common clay calcined at 800 °C (CRC), and fumed silica (SF).

Figure 1b shows a comparison between the mineralogical assemblage of precursors. MK presents muscovite and quartz as predominant minerals, accompanied by traces of anatase (TiO2, PDF#84-1286). As can be seen, the most significant differences between MK and CRC concern the contents of quartz (much reduced in MK) and amorphous material (much enhanced in MK considering the broad convexity located at 2θ~18–32°). SF was found to be completely amorphous, as already reported in previous works [17,48]. The high content of highly amorphous Si and the absence of major crystalline peaks justify the selection of SF as a secondary source of reactive silica in activated alkaline systems.

The chemical bulk compositions of MK, SF, and CRC are shown in Table 3. The most abundant oxides observed in the MK composition were silicon and aluminum oxides, related to the metakaolin content. These results agreed well with the product data sheet, albeit with a slightly lower content of Al_2O_3. Some variability in chemical composition can be easily attributed to the MK geological origin, and similar Al_2O_3 contents have been previously reported elsewhere for this commercial MK [56]. CRC was composed of similar SiO_2 and Al_2O_3 contents whereas major differences were found in alkaline oxides (Na_2O + K_2O), TiO_2, and Fe_2O_3. Such differences are in good agreement with the presence of alkali feldspars and anatase in the CRC mineralogical assemblage. The loss of ignition values in both calcined clays was inferior to 2.0 wt.%, which in part can be attributed to the thermal decomposition of muscovite.

Table 3. The chemical composition of the raw materials (% by mass).

	LOI *	SiO_2	Al_2O_3	CaO	Fe_2O_3	MgO	TiO_2	K_2O	Na_2O	Others
MK	1.9	57.0	34.5	0.2	1.2	0.2	1.8	0.4	nd*	2.9
CRC	1.2	56.0	33.9	0.2	4.2	0.5	0.4	3.4	0.1	0.3
SF	1.3	97.4	0.5	0.2	nd*	0.1	nd *	0.2	0.2	0.2

* LOI: loss on ignition, nd: less than quantification limit.

The particle size distribution of the precursors is provided in Figure 2. It can be seen that SF showed a coarser particle size distribution when compared with the remnant precursors. The calcined clays presented finer grain size distributions, with a smaller d10, d50, and d90 being found in CRC (Table 4). Among other factors, the precursors' particle size distribution determines the surface exposed to the alkaline medium, and thus influences the precursors' reactivity, the reaction kinetics, and the products formed. The finer particles of CRC precursors can possibly compensate to some extent for the lower degree of structural disorder and amorphous phases present in CRC when compared to MK (Figure 1b), thus resulting in precursors with potential akin to alkali activation technology. This mechanism seems to be corroborated by the strength and porosity results discussed in Section 3.2.6. In Figure 2 and Table 4, it can also be seen that the RC and CRC data points largely overlap with no significant differences being observed in the particle size distribution. Such similarity between the CRC and RC samples shows that the calcination process occurred without significant agglomeration of the clay particles, and thus without showing signs of sintering. It should be mentioned here that no grinding process was conducted after calcination to avoid mechanically imposed changes in the particle size distribution and reactivity, which would be intermingled in the interpretation of results. Overall, and despite the chemical, mineralogical, and physical differences regarding the benchmark precursor (MK), the results showed auspicious characteristics for the alkali activation of the examined local clays after calcification.

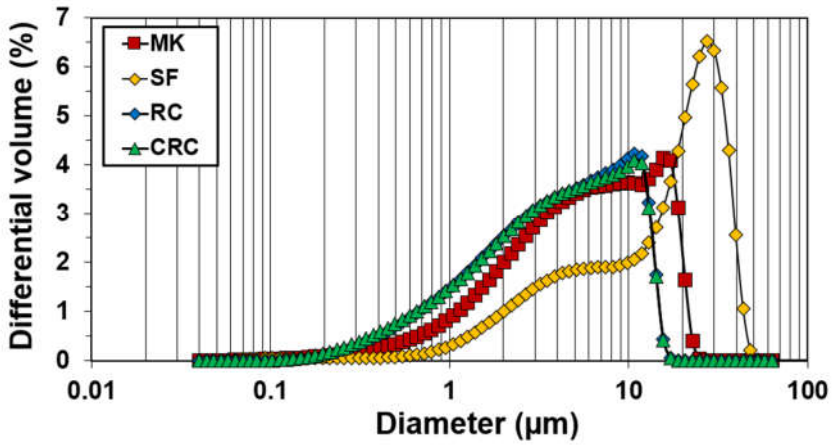

Figure 2. Particle size distribution of the precursors used to manufacture alkali activated binders and mortars: MK—commercial metakaolin; SF—silica fume; RC—as-received clay; CRC—calcined clay.

Table 4. The physical characteristics of the precursors.

Material	Mean Particle Size (μm)	D10 (μm)	D50 (μm)	D90 (μm)
MK	7.73	1.41	6.22	16.92
SF	18.11	2.70	17.77	35.16
RC	5.43	0.94	4.37	11.74
CRC	5.33	0.88	4.25	11.66

3.2. Alkali Activated Binders Characterization

3.2.1. Influence of Solid-to-Liquid Ratio

Compressive strength is among the most important properties of building materials as a measure of their load-bearing capacity, while density and porosity can be used as a proxy for durability. Figure 3 shows the apparent density (AD) and compressive strength (CS) of MK-binders produced with varying solid-to-liquid ratios (S/L ratio) while keeping other synthesis parameters constant (Table 1). After 7 days of curing, the SL0.90 samples recorded the highest CS values (9.8 ± 0.7 MPa) whereas SL1.00 showed the lowest CS (7.1 ± 1.2 MPa). The SL1.10 binders showed intermediate CS values of 9.2 ± 2.0 MPa but considerable standard deviations were recorded in all binders, which can be attributed to the specimens' early stage of maturation and ongoing polymerization reactions [17]. Later strength gains were observed in all binders, with SL1.00 being the most performant in terms of CS at 28 days. AP showed the opposite trend, with significant reductions being observed as curing progressed. Such reductions in AD can be mostly related to free water egress, as suggested by the linear relationship between solution load and AD at 28 days. Conversely, CS cannot be described as a linear function of the S/L ratio (nor of AD), as an inflection point appears to exist around a S/L ratio of 1.0. At a higher S/L ratio, AAM pastes presented a less workable consistency and increases in viscosity that could result in air entrapment within the structure in the samples. In fact, some air bubbles and minor voids were visible on the surface of the SL1.10 specimens, along with increases in the open porosity (OP) and water absorption (WA) values (Table 5). Increases in porosity can compromise SL1.10 stability and partially explain the reduced CS values observed. In addition, alkaline hydrolysis occurs at the interface between the alkaline media and solid particles (kaolinite minerals), and high S/L ratios can reduce diffusion, limit the degree of reaction, and ultimately reduce the binder formation. Reductions in CS were not, however, accompanied by reductions in AD, which were increased by the higher solid load existing in the SL1.10 systems. Conversely, lowering the S/L ratio to 0.90 yielded more workable pastes but resulted in less dense and mechanically resistant binders. In addition to the higher amount of free water in these systems, increased dosages of activating solution and Na^+ content that assist in dissolution may also hinder the polycondensation rate as the solid load available for reaction is limited and dispersed in a very fluid medium. The SL0.90 binders displayed limited CS increments from 7 to 28 days, not being able to outperform the SL1.0 samples. Therefore, the CS results suggest that SL1.00 binders allow for higher dissolution rates of the starting precursors while not hindering the polymerization reactions. Overall, all binders displayed sufficient CS for civil engineering applications and low AD values at 28 days that ranged from 1.28 ± 0.03 g/cm^3 to 1.36 ± 0.01 g/cm^3, whereas OPC pastes typically had AD greater than 1.80 g/cm^3. Considering these results, 1.00 was selected as the S/L ratio for further examination of the MK and CRC binders.

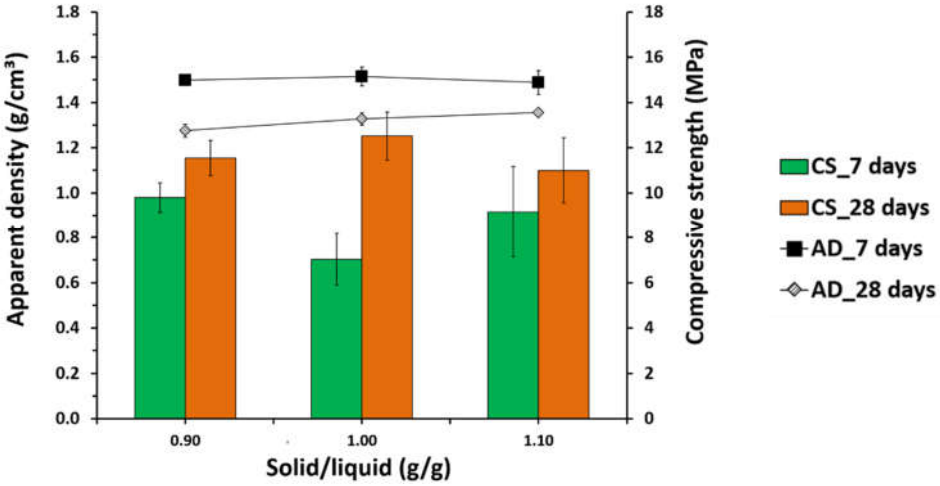

Figure 3. The apparent density and compressive strength of the alkali activated MK-binders at 7 and 28 days of curing as a function of the solid-to-liquid mass ratio.

Table 5. The water absorption and open porosity of the alkali activated binders after 28 days of curing.

	Water Absorption (WA)	**Open Porosity (OP)**
	%	%
SL0.90	15.68 ± 0.16	24.18 ± 0.17
SL1.00	14.34 ± 0.07	22.48 ± 0.15
SL1.10	14.96 ± 0.66	24.23 ± 1.09
CS4.00	14.34 ± 0.07	22.48 ± 0.15
CS3.50	14.35 ± 0.20	22.23 ± 0.37
CS3.00	14.45 ± 0.73	22.09 ± 0.91
HS1.50	14.34 ± 0.07	22.48 ± 0.15
HS1.25	15.47 ± 0.12	24.38 ± 0.16
HS1.00	15.51 ± 0.17	24.50 ± 0.38
M8	19.02 ± 0.27	29.36 ± 0.47
M10	14.34 ± 0.07	22.48 ± 0.15
M12	11.82 ± 0.28	18.56 ± 0.61
C1	14.34 ± 0.07	22.48 ± 0.15
C2	16.98 ± 0.22	27.90 ± 0.45
C3	15.16 ± 0.07	24.78 ± 0.24
R0	13.58 ± 0.72	21.81 ± 1.79
R25	14.27 ± 0.14	23.90 ± 0.15
R50	14.71 ± 0.82	24.08 ± 1.39
R75	13.00 ± 0.11	21.07 ± 0.20
R100	10.77 ± 0.16	17.54 ± 0.27

3.2.2. Influence of SF Incorporation

Given the insufficient availability of Si in the composition of some clay precursors, the addition of secondary sources of silica is often reported as necessary to deliver competent alkali-activated materials. The provision of extra silicon can be delivered by modifying the concentration and dosage of silicate solutions (discussed in Section 3.2.3) and/or

by introducing amorphous Si-rich powdered materials (e.g., silica fume) in partial lieu of clay precursors. However, optimal replacement levels vary according to the characteristics of the systems examined, thus requiring dedicated investigations as performed here.

Figure 4 shows the effects of MK replacement by SF on CS and AD. The results show that all binder formulations increased in CS and reduced in AD with curing, regardless of the MK to SF mass ratio (CC/SF ratio). After 28 days of curing, binders with the lowest CC/SF ratio (CS3.00) recorded the lowest CS values (10.1 ± 0.9 MPa), whereas the CS4.00 formulations showed the highest CS (12.5 ± 1.1 MPa). Oshani et al. [57] reported increases in CS up to 18 wt.% SF, but decreases for higher dosages. Previous studies have shown that excessive SF can be deleterious for CS development due to its volume expansion [58,59]. The authors reported that SF contents over 10 wt.% led to the formation of large voids and concomitant reductions in CS. However, residual modifications on AD, OP, and WA were imposed by the CC/SF ratio (Table 5), suggesting similar porous structures being formed in all binders. The highest early strength of the CS3.00 samples (8.2 ± 1.5 MPa; CS3.50 = 5.8 ± 0.7 MPa; CS4.00 = 7.1 ± 1.1 MPa) may indicate that SF promotes early age polymerization but hinders the later dissolution of clay precursors and/or the diffusion of dissolved species. However, increases in early CS can be an interesting technological feature if one is prepared to partially sacrifice strength development at later ages. Economic and environmental benefits can also accrue from the partial replacement of calcined clay by other Si-rich waste-based materials such as among others, rice husk ash, and the versatility and resilience introduced into the manufacturing process should also not be neglected here. Therefore, 3.00 was selected as the CC/SF ratio for the further examination of the MK and CRC binders.

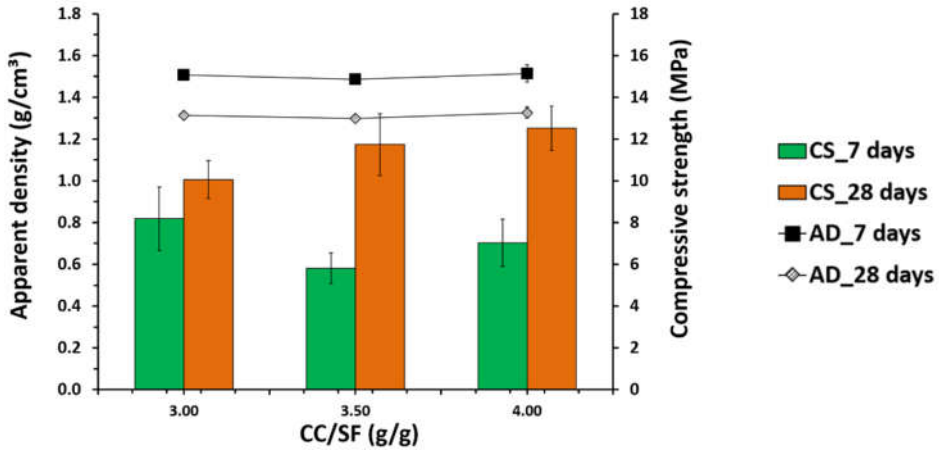

Figure 4. The apparent density and compressive strength of the alkali activated binders at 7 and 28 days of curing as a function of the calcined clay-to-silica fume mass ratio (CC/SF ratio).

3.2.3. Influence of NaOH-to-Na_2SiO_3 Ratio

Figure 5 shows the AD and CS of the binders produced with various NaOH-to-Na_2SiO_3 ratios by mass (SH/SS ratio), as per Table 1. The results showed that CS increased in all formulations with curing. AD showed the opposite trend but no noticeable differences were observed after 28 days of curing (≈1.32 g/cm³). Differences in WA and OP were also found to be residual, particularly between HS1.00 and HS1.25 binders (Table 5). However, the SH/SS ratio showed a considerable influence on strength development. After 7 days of curing, HS1.00 and HS1.25 recorded similar CS (≈10 MPa), whereas HS1.50 showed significantly lower values (7.1 ± 1.2 MPa). At later ages, CS was maximized at the SH/SS ratio of 1.00 (14.3 ± 1.6 MPa), with HS1.25 showing a CS similar to those of HS1.50 of 12.5 ± 2.0 MPa and 12.5 ± 1.0 MPa, respectively. These findings are in agreement with

previous results reported by, among others, Albidah et al. [60], Supit et al. [61], and Zhao et al. [62], who found increases in CS when reducing the SH/SS ratio. The authors also suggested the existence of the optimum SH/SS ratio below which further reductions will not deliver increases in strength. However, the existence of such a threshold limit cannot be inferred from the results discussed here. Increasing Na_2SiO_3 promoted the formation of more Si-rich structures, which contributed to the development of the highest CS in HS1.0. In addition, reducing the SH/SS ratio also decreased the activating solution pH, leading to more progressive dissolution and polycondensation, but ultimately allowing for higher reaction degrees [20]. It is interesting to point out the differences in the effects of introducing soluble silicates in the activating solution rather than as secondary powdered precursors (Section 3.2.2). In previous works [17], the authors demonstrated that using soluble silicates (K_2SiO_3) resulted in more densified structures and enhanced the mechanical performances. Although these effects can be largely determined by the precursor's composition and granulometric distribution, and by the concentration and nature of the silicate solutions (Na^+ vs. K^+), the results in Figure 5 recommend an SH/SS ratio of 1.00 to achieve the maximum CS values when synthesizing AAMs from CRC.

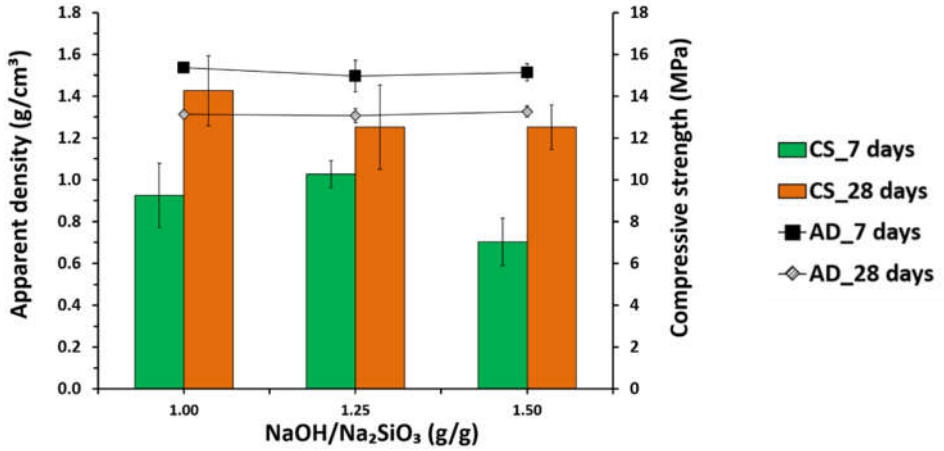

Figure 5. The apparent density and compressive strength of the alkali activated binders at 7 and 28 days of curing as a function of the sodium hydroxide-to-sodium silicate mass ratio.

It should be mentioned that silicate solutions entail significant production costs and environmental burdens [20,21,63] and restrictions in the Na_2SiO_3 dosage should be considered in the following optimization studies, if technologically possible.

3.2.4. Influence of NaOH Molarity

Figure 6 presents the CS and AD of the MK-binders activated with the Na_2SiO_3 and NaOH solutions, in which the molarity of the latter was 8 M, 10 M, or 12 M (Table 1). The influence of NaOH molarity on CS development is notorious. Yearly age CS ranged between 2.7 ± 0.7 MPa (M8) and 12.2 ± 1.5 MPa (M12), being greatly proportional to the NaOH molarity. At 28 days, NaOH 8 M solutions delivering binders with CS did not exceed 3.4 ± 0.7 MPa, whereas the M10 and M12 binders displayed CS values around 12.5 MPa. The results suggest that in these systems, the optimal alkali environment for MK activation requires NaOH solutions with a minimum molarity of 10 M, if CS values higher than 10 MPa are to be attained. If sufficient alkalinity is not provided, MK dissolution may be partially impaired and the degree of polymerization of the final products may be weakened. Conversely to what was previously suggested [60–62], no inflection point was observed in CS when increasing the Na^+ availability. An excess of hydroxide ions and the deleterious formation of Na_2CO_3 did not seem to exist to a large extent as no efflorescence

was visible on the surfaces of the M10 and M12 samples. AD was reduced in all binders with curing, but after 28 days, the M12 binders were slightly denser. It is also interesting to note that the WA and OP values increased as the NaOH molarity decreased, even at similar AD values (Table 5). This may suggest modifications in the pore connectivity and tortuosity favored by higher Na^+ availability. For better understanding of the morphology, distribution, and connectivity of pores, microstructural analysis and BET analysis can be suggested and will pursued in future works. Reducing the NaOH molarity, and thus the $(Na_2O + K_2O)/SiO_2$ molar ratio, also slightly enhanced the binders' viscosity and workability, but 12 M solutions were selected for further experimentation to maximize the yearly CS in the CRC binders.

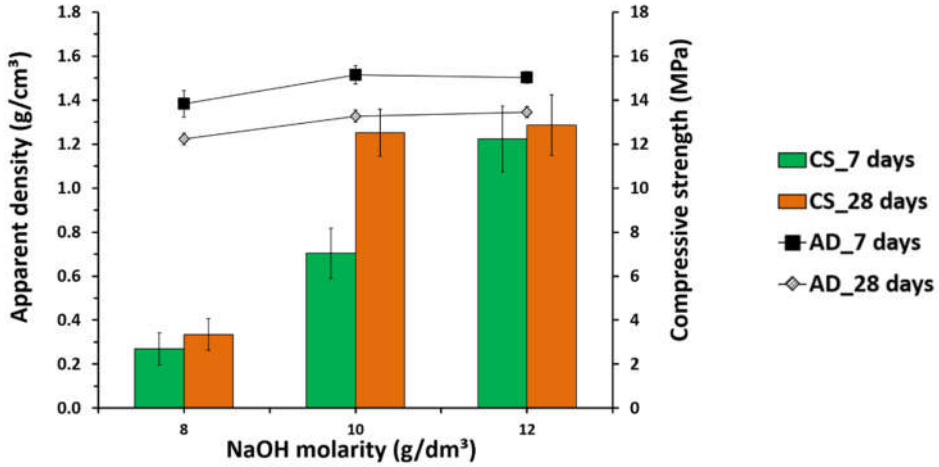

Figure 6. The apparent density and compressive strength of the alkali activated binders at 7 and 28 days of curing as a function of sodium hydroxide molarity.

3.2.5. Effect of Curing Conditions

Different curing conditions were evaluated and their effects on the binder properties were examined to define the optimum mix designs. At curing conditions 1 and 2, the specimens were cured at slightly elevated temperatures (40 °C) for a 24 h period, albeit starting immediately after mixing or 24 h later, C1 and C2, respectively. When employing curing condition 3 (C3), heat curing was initiated as in C2, but maintained for a 5 day period. In short, C1–C2 served to investigate the effects associated with heat curing location in time, while C2–C3 determined its most adequate duration for the systems examined here. Figure 7 describes the AD and CS of the binders cured with different curing regimes. After 28 days, the C3 samples recorded the highest AD (1.39 ± 0.02 g/cm³) and CS values (13.6 ± 1.2 MPa). C1 and C2 showed a CS within the experimental error range (12.5 ± 1.1 MPa and 12.1 ± 1.9 MPa, respectively), and a slightly higher AD was observed in the C2 samples of 1.35 ± 0.02 g/cm³ (C1 = 1.33 ± 0.03 g/cm³). In addition, the yearly age CS was considerably ameliorated with the increment of the curing period (C2–C3) and benefitted from a dormant period in the initial stage of the reaction (C1–C2). Increases in AD and CS indicate highly polymerized and resistant structures being formed in C3, which, however, cannot be related to the densification and reduction in porosity (Table 5). Similar findings have previously been reported on slag-based systems where the benefits of curing at a slightly elevated temperature with an initial dormant period were demonstrated [17,32,38]. The volumetric stability of the specimens was not determined, but pronounced shrinkage phenomena able to provoke visible cracks and severely compromise CS did not seem to exist. The higher CS and AD values found in the C3 binders justify the selection

of the C3 conditions for further experimentation when replacing MK with the CRC precursors.

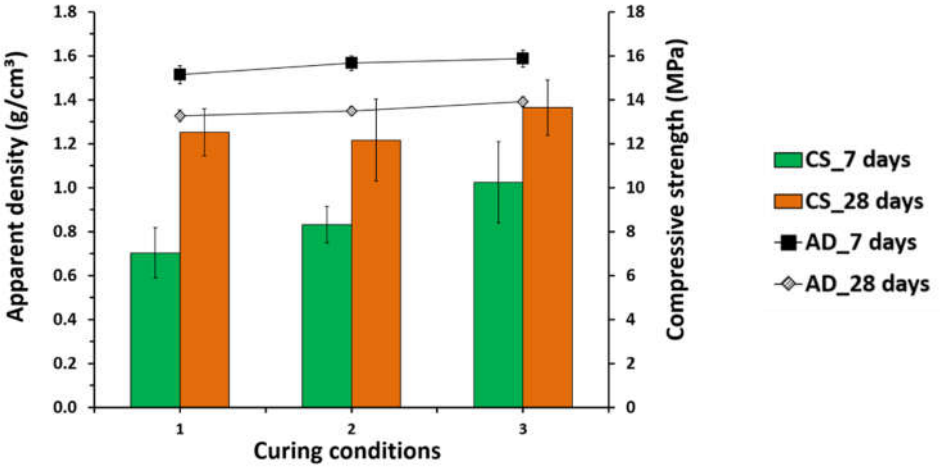

Figure 7. The apparent density and compressive strength of the alkali activated binders at 7 and 28 days of curing as a function of the curing conditions used as per Table 2.

3.2.6. Influence of CRC Incorporation

In Sections 3.2.1–3.2.5, the baseline MK system was investigated and the optimal synthesis conditions were selected. A binder synthesized with the S/L = 1.0, C/S = 3.0, SH/SS = 1.0, NaOH molarity = 12 M, and cured in C3 conditions (Table 1) was defined as the reference binder (R0; 0.0 wt.% CRC) to investigate the effects of MK replacement by CRC. Figure 8 presents the representative photographs of the alkali activated binders produced with the progressive replacement of MK by CRC (0, 25, 50, 75, and 100 wt.%).

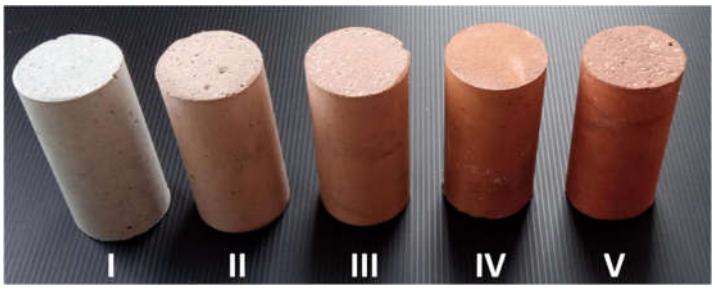

Figure 8. Representative photographs of the alkali activated binders produced with the progressive replacement of MK by CRC. From left to right: (i) 0.0%, (ii) 25.0%, (iii) 50.0%, (iv) 75.0%, and (v) 100.0% MK replacement.

Figure 9 shows the AD and CS of the binders with varying CRC dosages after 7 and 28 days of curing. Residual increases in AD could be seen as the CRC content rose (AD_{28dmin}, R0 = 1.37 ± 0.02 g/cm^3; AD_{28dmax}, R100 = 1.45 ± 0.01 g/cm^3), which can be attributed to the presence of iron in the CRC composition. CRC incorporation levels up to 75 wt.% resulted in slight increases in the yearly age CS. An optimal replacement level seemed to exist around 50 wt.% CRC, where the R50 samples recorded the highest CS values after 7 days of curing (12.5 ± 0.7 MPa), representing a 32.6% increase in comparison to the pure MK-binders (Figure 9). MK total replacement by CRC seemed to have no deleterious effects on early CS, but considerably increased the mechanical performance after 28 days of curing. Curiously, as the CRC content rises, the theoretical $SiO_2/(Al_2O_3 + Fe_2O_3)$ molar ratio

of the mixtures decreases, thus less polymerized structures would be expected. Differences in the reaction rates arising from the CRC particle size distribution and composition (as discussed in Section 3.1) can explain to some extent the late strength developments in the R100 binders, but do not provide a general definition for the trends observed in the CS nor the WA and OP results.

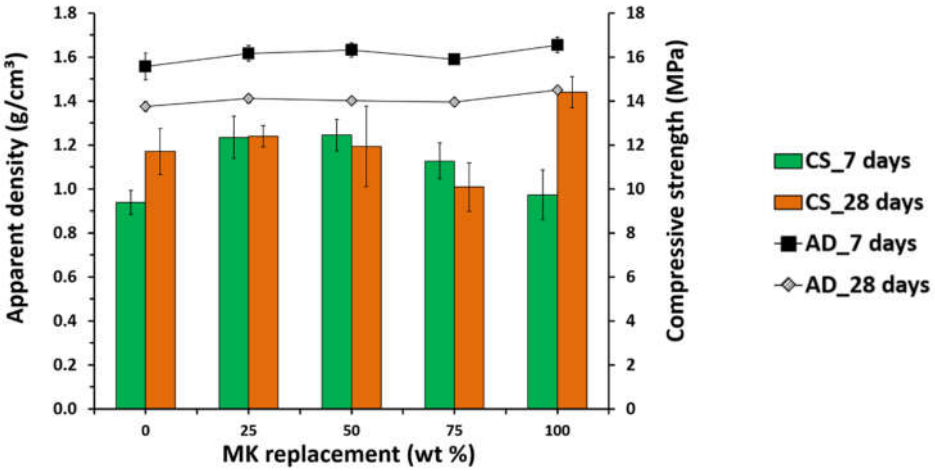

Figure 9. The apparent density and compressive strength of the alkali activated binders at 7 and 28 days of curing as a function of metakaolin replacement by calcined common clay.

Therefore, the mineralogical differences were investigated by means of XRD and the diffraction analysis of the binders prepared with the progressive replacement of MK by CRC (0, 50 and 100%) is shown in Figure 10. Amorphous material (broad convexity located at 2θ~22–35°) could be appreciated in all cases, which confirmed polymerization, even when totally replacing MK with CRC. The differences in the intensity of the quartz peaks found in the starting materials remained after alkali activation, but they appeared as much less remarkable. The dissolution of quartz from CRC is consistent with the increase in the relative intensity between the main peaks of microcline (PDF#77-0135) and quartz (PDF#87-0743). However, some crystalline quartz persisted, showing that some Si units did not partake in the reactions. Muscovite (PDF#80-0743) was detected in both the MK and CRC-containing binders, and anhydrous aluminum silicate phases ($Al_{0.5}Si_{0.75}O_{2.25}$, PDF#37-1480) identified in CRC precursors could not be detected, suggesting their dissolution and participation in polymerization reactions. The contribution of these phases can explain the porosity values and CS increases to some extent, but dedicated studies are still needed to better understand the composition and morphology of the reaction products that formed to provide a discretionary explanation of the reaction mechanisms involved.

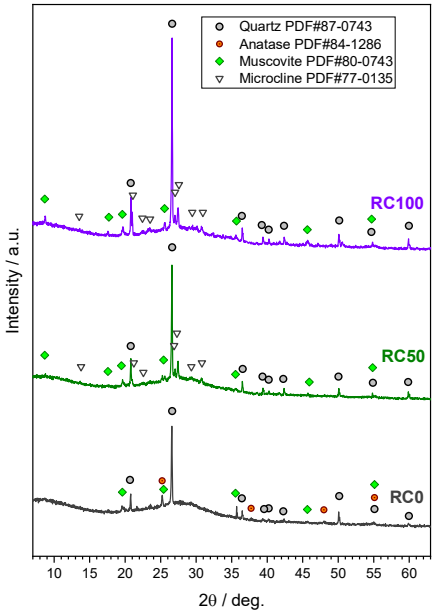

Figure 10. A comparison between the XRD patterns of the binders synthesized with progressive replacement (0, 50, and 100%) of metakaolin by local calcined clay after 28 days of curing.

3.3. Alkali Activated Mortars

Mortar samples were produced and characterized to preliminarily assess the practical interest and industrial feasibility of the developed CRC binders. Fundamental properties evaluated in a fresh state included fresh density and workability. The workability of the mortars was investigated by the flow table test. The spread values were slightly reduced with the increment in the CRC content in the mix design (Table 6). However, all of the results are in line with the spread values used in regular hydraulic mortars (non-self-leveling/self-compacting) that typically lie in the range of 150–180 mm. Therefore, all mortars demonstrated adequate workability levels without the use of any additional additives and could meet the standard flowability requirements. The fresh density values were nearly constant, albeit slightly higher values were observed in the MR100 mortars. This effect was even more pronounced in the AD values at 28 days. The polymerization reaction seems to dictate the unit weight with progressive increases in fresh density and AD as the CRC dose rises (MR100, AD $_{28dmax}$ = 1.99 ± 0.01 MPa).

Table 6. The fresh and hardened properties of mortars produced with different dosages of local calcined clays at 28 days.

Code	SV (mm)*	FD (g/cm³)*	AD (g/cm³)*	EM (GPa)*	WA (%)*	CI*
MR0	180 ± 5	2.01	1.78 ± 0.00	15.4 ± 0.0	6.7 ± 0.0	0.118± 0.002
MR25	175 ± 5	1.99	1.85 ± 0.02	16.8 ± 0.2	7.0 ± 0.3	0.138 ± 0.002
MR50	175 ± 10	2.01	1.88 ± 0.07	16.3 ± 0.5	7.5 ± 0.3	0.120 ± 0.007
MR75	175 ± 5	2.00	1.91 ± 0.01	16.8 ± 0.1	4.1 ± 0.7	0.128 ± 0.006
MR100	170 ± 5	2.05	1.99 ± 0.01	14.7 ± 0.1	3.0 ± 0.2	0.101 ± 0.000

* Properties abbreviate as: SV—spread value; FD—fresh density; EM—elastic modulus; WA—water absorption; CP—capillarity index.

As with the binders, CS and OP were the utmost important properties that must be investigated in AAM mortars. Figure 11 describes the relationship between the CS and OP levels in mortars produced with progressive dosages of CRC. The CS values decreased almost linearly as the CRC increased. Interestingly, a similar trend was not observed in the CRC binders (Figure 8), suggesting aggregate interference in the polymerization

reactions/products and/or structural weaknesses located in the interfacial transition zones. The OP increased slightly with an increasing CRC up to 50 wt.%, but beyond this threshold, considerable decreases were observed. The values for the WA and elastic modulus were greatly affected by pores and voids, following, in general, a pattern similar to that observed for OP (Table 6). The capillarity index values were found to be inconsistent and without any visible correlation to other properties. Therefore, the relationships between the density, porosity, CRC content, and strength development in the CRC mortars seem much more intricate with respect to the binders only, and effectively rely on a larger number of complex reactions and confounding variables. In Figure 11, the existence of three distinct zones is enunciated based on the MK replacement level. In zone 1, the increases in porosity seemed to be partially mitigated by the formation of slightly more resistant binders, while in zone 2, the exact opposite seemed to happen, but to a lesser extent. In zone 3, the motifs that led to mortars with denser structures and produced from binders more resistant to develop poorer mechanical performances are still unclear at this point and will be the subject of research in future works. However, all mortars produced presented low OP and WA (below 15% and 8%, respectively) and CS values above 28 MPa, which provide good performance indicators regarding their mechanical behavior and durability and well illustrates their potential for applications in construction.

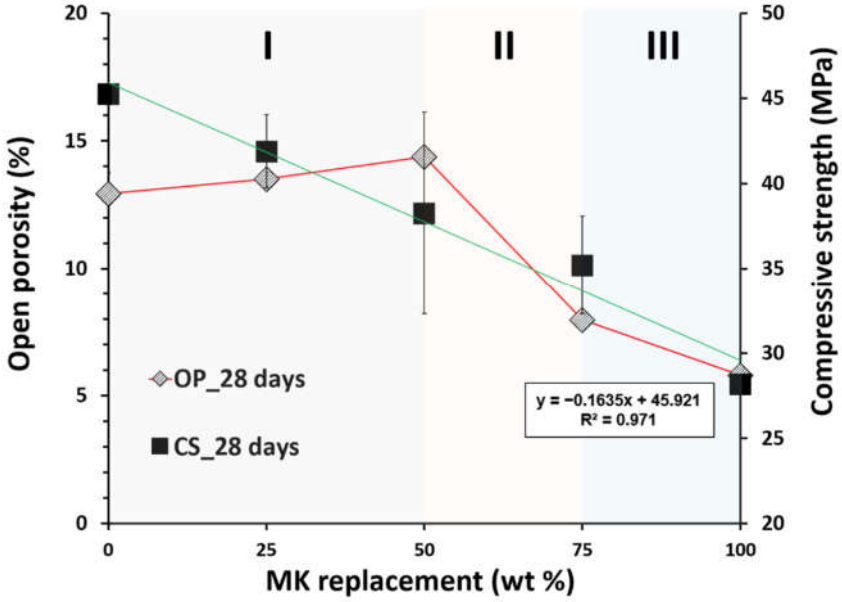

Figure 11. A comparison of the open porosity and compressive strength values of mortars produced with the progressive replacement of metakaolin by local calcined clays after 28 days of curing. I, II and III indicate ranges of MK replacement levels with different relationships between open porosity and compressive strength.

4. Conclusions

In this work, the factors affecting the properties of the alkali activated binders and mortars produced from different thermally modified clays were investigated. Commercial metakaolin was taken as the benchmark clay precursor and an endogenous common clay was explored as a representative example of potential local alternatives for greater environmental and economic benefits. The resulting MK binders showed compressive strengths above 10 MPa, low density (AD > 1.40 g/cm^3), and low OP and WA values (30% and 20%, respectively) after 28 days of curing. Replacing MK with locally available clays was found to be feasible as the key fundamental properties were maintained at levels comparable to those of the reference system, thus making the mortars produced thereof

(spread >170 mm; CS >28 MPa; 1.78 g/cm^3 > AD > 1.99 g/cm^3; OP >15%; WA >8%) potentially viable candidates for various applications in construction, rehabilitation, and architectural works. The results obtained in this study also showed that clay-based AAMs exhibit adaptable properties and that resilient manufacturing processes can be designed by proper control of the mix design, for example, MK and CRC can be alternated as the main aluminosilicate source, whereas additional Si can be delivered either by the addition of Na_2SiO_3 or silica fume without major deleterious effects. A prolonged curing period at slightly elevated temperatures is recommended for yielding the maximum strength results.

Overall, the results shown here demonstrate that novel building materials can be produced from an as yet unexplored myriad of common clay resources, thus making an initial contribution to the development of more sustainable manufacturing practices. This work also aimed to shed light on emergent clay binders to stimulate further new scientific developments and industrial advances in clay activation technology with the meaningful co-creation of economic and environmental added value in the region.

Author Contributions: Conceptualization, G.A.; Methodology, G.A.; Validation, G.A.; Formal analysis, G.A. and E.B.; Investigation, G.A.; Resources V.M.F.; Data curation, G.A; Writing—original draft preparation, G.A.; Writing—review and editing, G.A., E.B., and V.M.F.; Visualization, G.A.; Funding acquisition, V.M.F. All authors have read and agreed to the published version of the manuscript.

Funding: This research work was also supported by the Foundation for Science and Technology (FCT)—Aveiro Research Center for Risks and Sustainability in Construction (RISCO), Universidade de Aveiro, Portugal [FCT/UIDB/ECI/04450/2020]. This publication reflects only the authors' views, exempting the funding agency from any liability.

Institutional Review Board Statement: Not applicable.

Informed Consent Statement: Not applicable.

Data Availability Statement: The data presented in this study are available on request from the corresponding author.

Acknowledgments: The authors wish to thank Rui M. Novais and João Carvalheiras for their assistance during the clay calcination protocols and analytical testing.

Conflicts of Interest: The authors declare no conflicts of interest. The funders had no role in the design of the study; in the collection, analyses, or interpretation of data; in the writing of the manuscript, or in the decision to publish the results

References

1. EPA USA. Inventory of U.S. Greenhouse Gas Emissions and Sinks. 8 February 2017. Available online: https://www.epa.gov/ghgemissions/inventory-us-greenhouse-gas-emissions-and-sinks (accessed on 8 June 2022).
2. Habert, G.; Miller, S.A.; John, V.M.; Provis, J.L.; Favier, A.; Horvath, A.; Scrivener, K.L. Environmental impacts and decarbonization strategies in the cement and concrete industries. *Nat. Rev. Earth Environ.* **2020**, *1*, 559–573. https://doi.org/10.1038/s43017-020-0093-3.
3. Scrivener, K.L.; John, V.M.; Gartner, E.M. Eco-efficient cements: Potential economically viable solutions for a low-CO2 cement-based materials industry. *Cem. Concr. Res.* **2018**, *114*, 2–26. https://doi.org/10.1016/j.cemconres.2018.03.015.
4. Abergel, T.; Dean, B.; Dulac, J.; Hamilton, I.; Wheeler, T. Global Status Report: Towards a Zero-Emission, Efficient and Resilient Buildings and Construction Sector. 2018. Available online: https://www.worldgbc.org/sites/default/files/2018%20GlobalABC%20Global%20Status%20Report.pdf(accessed on 10 June 2022).
5. Favier, A.; De Wolf, C.; Scrivener, K.; Habert, G. *A Sustainable Future for the European Cement and Concrete Industry: Technology Assessment for Full Decarbonisation of the Industry by 2050*; ETH Zurich: Zurich, Switzerland, 2018.
6. Amran, M.; Debbarma, S.; Ozbakkaloglu, T. Fly ash-based eco-friendly geopolymer concrete: A critical review of the long-term durability properties. *Constr. Build. Mater.* **2021**, *270*, 121857. https://doi.org/10.1016/j.conbuildmat.2020.121857.
7. Gartner, E.; Sui, T. Alternative cement clinkers. *Cem. Concr. Res.* **2018**, *114*, 27–39. https://doi.org/10.1016/j.cemconres.2017.02.002.
8. Hertel, T.; Van den Bulck, A.; Onisei, S.; Sivakumar, P.P.; Pontikes, Y. Boosting the use of bauxite residue (red mud) in cement—Production of an Fe-rich calciumsulfoaluminate-ferrite clinker and characterisation of the hydration. *Cem. Concr. Res.* **2021**, *145*, 106463. https://doi.org/10.1016/j.cemconres.2021.106463.

9. Ribeiro, F.R.C.; Modolo, R.C.E.; Kulakowski, M.P.; Brehm, F.A.; Moraes, C.A.M.; Ferreira, V.M.; Mesquita, E.F.T.; de Azevedo, A.R.G.; Monteiro, S.N. Production of Belite Based Clinker from Ornamental Stone Processing Sludge and Calcium Carbonate Sludge with Lower CO2 Emissions. *Materials* **2022**, *15*, 2352. https://doi.org/10.3390/ma15072352.
10. Sabbah, A.; Zhutovsky, S. Effect of sulfate content and synthesis conditions on phase composition of belite-ye'elimite-ferrite (BYF) clinker. *Cem. Concr. Res.* **2022**, *155*, 106745. https://doi.org/10.1016/j.cemconres.2022.106745.
11. Tan, B.; Okoronkwo, M.U.; Kumar, A.; Ma, H. Durability of calcium sulfoaluminate cement concrete. *J. Zhejiang Univ. Sci. A* **2020**, *21*, 118–128. https://doi.org/10.1631/jzus.A1900588.
12. Meyer, V.; de Cristofaro, N.; Bryant, J.; Sahu, S. Solidia Cement an Example of Carbon Capture and Utilization. *Key Eng. Mater.* **2018**, *761*, 197–203. https://doi.org/10.4028/www.scientific.net/KEM.761.197.
13. Bishnoi, S. *Calcined Clays for Sustainable Concrete*, Springer: Berlin/Heidelberg, Germany, 2019.
14. Dhandapani, Y.; Joseph, S.; Bishnoi, S.; Kunther, W.; Kanavaris, F.; Kim, T.; Irassar, E.; Castel, A.; Zunino, F.; Machner, A.; et al. Durability performance of binary and ternary blended cementitious systems with calcined clay: A RILEM TC 282 CCL review. *Mater. Struct.* **2022**, *55*, 145. https://doi.org/10.1617/s11527-022-01974-0.
15. Ez-zaki, H.; Marangu, J.M.; Bellotto, M.; Dalconi, M.C.; Artioli, G.; Valentini, L. A Fresh View on Limestone Calcined Clay Cement (LC3) Pastes. *Materials* **2021**, *14*, 3037. https://doi.org/10.3390/ma14113037.
16. Sharma, M.; Bishnoi, S.; Martirena, F.; Scrivener, K. Limestone calcined clay cement and concrete: A state-of-the-art review. *Cem. Concr. Res.* **2021**, *149*, 106564. https://doi.org/10.1016/j.cemconres.2021.106564.
17. Ascensão, G.; Marchi, M.; Segata, M.; Faleschini, F.; Pontikes, Y. Reaction kinetics and structural analysis of alkali activated Fe–Si–Ca rich materials. *J. Clean. Prod.* **2020**, *246*, 119065. https://doi.org/10.1016/j.jclepro.2019.119065.
18. Novais, R.M.; Pullar, R.C.; Labrincha, J.A. Geopolymer foams: An overview of recent advancements. *Prog. Mater. Sci.* **2020**, *109*, 100621. https://doi.org/10.1016/j.pmatsci.2019.100621.
19. Palomo, A.; Maltseva, O.; Garcia-Lodeiro, I.; Fernández-Jiménez, A. Portland Versus Alkaline Cement: Continuity or Clean Break: "A Key Decision for Global Sustainability". *Front. Chem.* **2021**, *9*, 705475. https://doi.org/10.3389/fchem.2021.705475.
20. Abdulkareem, M.; Havukainen, J.; Nuortila-Jokinen, J.; Horttanainen, M. Environmental and economic perspective of waste-derived activators on alkali-activated mortars. *J. Clean. Prod.* **2021**, *280*, 124651. https://doi.org/10.1016/j.jclepro.2020.124651.
21. Abdulkareem, M.; Havukainen, J.; Horttanainen, M. How environmentally sustainable are fibre reinforced alkali-activated concretes? *J. Clean. Prod.* **2019**, *236*, 117601. https://doi.org/10.1016/j.jclepro.2019.07.076.
22. Fořt, J.; Mildner, M.; Keppert, M.; Černý, R. Waste solidified alkalis as activators of aluminosilicate precursors: Functional and environmental evaluation. *J. Build. Eng.* **2022**, *54*, 104598. https://doi.org/10.1016/j.jobe.2022.104598.
23. Habert, G.; Ouellet-Plamondon, C. Recent update on the environmental impact of geopolymers. *RILEM Tech. Lett.* **2016**, *1*, 17. https://doi.org/10.21809/rilemtechlett.2016.6.
24. Mascarin, L.; Ez-zaki, H.; Garbin, E.; Bediako, M.; Valentini, L. Mitigating the ecological footprint of alkali-activated calcined clays by waste marble addition. *Cem. Concr. Compos.* **2022**, *127*, 104382. https://doi.org/10.1016/j.cemconcomp.2021.104382.
25. Djobo, J.N.Y.; Elimbi, A.; Tchakouté, H.K.; Kumar, S. Volcanic ash-based geopolymer cements/concretes: The current state of the art and perspectives. *Environ. Sci. Pollut. Res.* **2017**, *24*, 4433–4446. https://doi.org/10.1007/s11356-016-8230-8.
26. Hamid, M.A.; Yaltay, N.; Türkmenoğlu, M. Properties of pumice-fly ash based geopolymer paste. *Constr. Build. Mater.* **2022**, *316*, 125665. https://doi.org/10.1016/j.conbuildmat.2021.125665.
27. Tan, J.; Dan, H.; Ma, Z. Metakaolin based geopolymer mortar as concrete repairs: Bond strength and degradation when subjected to aggressive environments. *Ceram. Int.* **2022**, *48*, 23559–23570. https://doi.org/10.1016/j.ceramint.2022.05.004.
28. Novais, R.M.; Ascensão, G.; Seabra, M.P.; Labrincha, J.A. Waste glass from end-of-life fluorescent lamps as raw material in geopolymers. *Waste Manag.* **2016**, *52*, 245–255. https://doi.org/10.1016/j.wasman.2016.04.003.
29. Ascensão, G.; Seabra, M.P.; Aguiar, J.B.; Labrincha, J.A. Red mud-based geopolymers with tailored alkali diffusion properties and pH buffering ability. *J. Clean. Prod.* **2017**, *148*, 23–30. https://doi.org/10.1016/j.jclepro.2017.01.150.
30. Giels, M.; Hertel, T.; Gijbels, K.; Schroeyers, W.; Pontikes, Y. High performance mortars from vitrified bauxite residue; the quest for the optimal chemistry and processing conditions. *Cem. Concr. Res.* **2022**, *155*, 106739. https://doi.org/10.1016/j.cemconres.2022.106739.
31. Arnout, L.; Beersaerts, G.; Liard, M.; Lootens, D.; Pontikes, Y. Valorising Slags from Non-ferrous Metallurgy into Hybrid Cementitious Binders: Mix Design and Performance. *Waste Biomass Valorization* **2021**, *12*, 4679–4694. https://doi.org/10.1007/s12649-020-01322-9.
32. Ascensão, G.; Beersaerts, G.; Marchi, M.; Segata, M.; Faleschini, F.; Pontikes, Y. Shrinkage and Mitigation Strategies to Improve the Dimensional Stability of $CaO\text{-}FeO_x\text{-}Al2O_3\text{-}SiO_2$ Inorganic Polymers. *Materials* **2019**, *12*, 3679. https://doi.org/10.3390/ma12223679.
33. Klima, K.M.; Schollbach, K.; Brouwers, H.J.H.; Yu, Q. Thermal and fire resistance of Class F fly ash based geopolymers—A review. *Constr. Build. Mater.* **2022**, *323*, 126529. https://doi.org/10.1016/j.conbuildmat.2022.126529.
34. Li, X.; Bai, C.; Qiao, Y.; Wang, X.; Yang, K.; Colombo, P. Preparation, properties and applications of fly ash-based porous geopolymers: A review. *J. Clean. Prod.* **2022**, *359*, 132043. https://doi.org/10.1016/j.jclepro.2022.132043.
35. Novais, R.M.; Ascensão, G.; Tobaldi, D.M.; Seabra, M.P.; Labrincha, J.A. Biomass fly ash geopolymer monoliths for effective methylene blue removal from wastewaters. *J. Clean. Prod.* **2018**, *171*, 783–794. https://doi.org/10.1016/j.jclepro.2017.10.078.
36. Novais, R.M.; Buruberri, L.H.; Ascensão, G.; Seabra, M.P.; Labrincha, J.A. Porous biomass fly ash-based geopolymers with tailored thermal conductivity. *J. Clean. Prod.* **2016**, *119*, 99–107. https://doi.org/10.1016/j.jclepro.2016.01.083.

37. Rakhimova, N.R. A review of calcined clays and ceramic wastes as sources for alkali-activated materials. *Geosystem Eng.* **2020**, *23*, 287–298. https://doi.org/10.1080/12269328.2020.1768154.
38. Beersaerts, G.; Ascensão, G.; Pontikes, Y. Modifying the pore size distribution in Fe-rich inorganic polymer mortars: An effective shrinkage mitigation strategy. *Cem. Concr. Res.* **2021**, *141*, 106330. https://doi.org/10.1016/j.cemconres.2020.106330.
39. Ferone, C.; Liguori, B.; Capasso, I.; Colangelo, F.; Cioffi, R.; Cappelletto, E.; Di Maggio, R. Thermally treated clay sediments as geopolymer source material. *Appl. Clay Sci.* **2015**, *107*, 195–204. https://doi.org/10.1016/j.clay.2015.01.027.
40. Khalifa, A.Z.; Pontikes, Y.; Elsen, J.; Cizer, Ö. Comparing the reactivity of different natural clays under thermal and alkali activation. *RILEM Tech. Lett.* **2019**, *4*, 74–80. https://doi.org/10.21809/rilemtechlett.2019.85.
41. Valentini, L.; Mascarin, L.; Dalconi, M.C.; Garbin, E.; Ferrari, G.; Artioli, G. Performance and Properties of Alkali-Activated Blend of Calcined Laterite and Waste Marble Powder. In *Calcined Clays for Sustainable Concrete*; Bishnoi, S., Ed.; RILEM Bookseries; Springer: Singapore, 2020; Volume 25, pp. 375–380; ISBN 9789811528057.
42. Valentini, L.; Mascarin, L. Assessing the dimensional stability of alkali-activated calcined clays in the fresh state: A time-lapse X-ray imaging approach. *Mater. Struct.* **2021**, *54*, 35. https://doi.org/10.1617/s11527-021-01623-y.
43. Khalifa, A.Z.; Cizer, Ö.; Pontikes, Y.; Heath, A.; Patureau, P.; Bernal, S.A.; Marsh, A.T.M. Advances in alkali-activation of clay minerals. *Cem. Concr. Res.* **2020**, *132*, 106050. https://doi.org/10.1016/j.cemconres.2020.106050.
44. Lopes, C.; Lisboa, V.; Carvalho, J.; Mateus, A.; Martins, L. Challenges to access and safeguard mineral resources for society: A case study of kaolin in Portugal. *Land Use Policy* **2018**, *79*, 263–284. https://doi.org/10.1016/j.landusepol.2018.07.035.
45. Reichl, C.; Schatz, M.; Zsak, G. World Mining Data 2018 Iron and Ferro Alloy Metals Non-Ferrous Metals Precious Metals Industrial Minerals Mineral Fuels. 2018. Available online: https://www.world-mining-data.info/wmd/downloads/PDF/WMD2018.pdf (accessed on 28 June 2022).
46. Peys, A.; White, C.E.; Rahier, H.; Blanpain, B.; Pontikes, Y. Alkali-activation of CaO-FeOx-SiO2 slag: Formation mechanism from in-situ X-ray total scattering. *Cem. Concr. Res.* **2019**, *122*, 179–188. https://doi.org/10.1016/j.cemconres.2019.04.019.
47. Simon, S.; Gluth, G.J.G.; Peys, A.; Onisei, S.; Banerjee, D.; Pontikes, Y. The fate of iron during the alkali-activation of synthetic (CaO-)FeOx-SiO2 slags: An Fe K -edge XANES study. *J. Am. Ceram. Soc.* **2018**, *101*, 2107–2118. https://doi.org/10.1111/jace.15354.
48. Ascensão, G.; Faleschini, F.; Marchi, M.; Segata, M.; Van De Sande, J.; Rahier, H.; Bernardo, E.; Pontikes, Y. High-Temperature Behavior of CaO-FeOx-Al2O3-SiO2-Rich Alkali Activated Materials. *Appl. Sci.* **2022**, *12*, 2572. https://doi.org/10.3390/app12052572.
49. *EN 1015-11:2019*; Methods of Test for Mortar for Masonry—Part 11: Determination of Flexural and Compressive Strength of Hardened Mortar. European Committee for Standardization: Brussels, Belgium, 2019.
50. ASTM International. Standard Test Method for Obtaining and Testing Drilled Cores and Sawed Beams of Concrete. Available online: https://www.astm.org/c0042_c0042m-12.html (accessed on 15 July 2022).
51. *EN 1015-3*; Methods of Test for Mortar for Masonry—Part 3: Determination of Consistence of Fresh Mortar (by Flow Table). European Committee for Standardization: Brussels, Belgium, 2007. Available online: https://www.en-standard.eu/din-en-1015-3-methods-of-test-for-mortar-for-masonry-part-3-determination-of-consistence-of-fresh-mortar-by-flow-table-includes-amendments-a1-2004-a2-2006/ (accessed on 15 July 2022).
52. *EN 1015-6*; Methods of Test for Mortar for Masonry Determination of Bulk Density of Fresh Mortar. European Committee for Standardization: Brussels, Belgium, 2007. Available online: https://www.en-standard.eu/search/?q=EN+1015-6 (accessed on 15 July 2022).
53. *EN 12504-4*; Testing Concrete in Structures—Part 4: Determination of Ultrasonic Pulse Velocity. European Committee for Standardization: Brussels, Belgium, 2021. Available online: https://www.en-standard.eu/csn-en-12504-4-testing-concrete-in-structures-part-4-determination-of-ultrasonic-pulse-velocity/ (accessed on 29 July 2022).
54. *EN 1015-18:2002*; Methods of Test for Mortar for Masonry Determination of Water Absorption Coefficient Due to Capillary Action of Hardened Mortar. European Committee for Standardization: Brussels, Belgium, 2002. Available online: https://www.en-standard.eu/bs-en-1015-18-2002-methods-of-test-for-mortar-for-masonry-determination-of-water-absorption-coefficient-due-to-capillary-action-of-hardened-mortar/ (accessed on 15 July 2022).
55. Merabtene, M.; Kacimi, L.; Clastres, P. Elaboration of geopolymer binders from poor kaolin and dam sludge waste. *Heliyon* **2019**, *5*, e01938. https://doi.org/10.1016/j.heliyon.2019.e01938.
56. Ferraz, E.; Andrejkovičová, S.; Hajjaji, W.; Velosa, A.L.; Silva, A.S.; Rocha, F. Pozzolanic activity of metakaolins by the French standard of the modified Chapelle test: A direct methology. *Acta Geodyn. Geomater.* **2015**, *12*, 289–298. https://doi.org/10.13168/AGG.2015.0026.
57. Oshani, F.; Allahverdi, A.; Kargari, A.; Norouzbeigi, R.; Mahmoodi, N.M. Effect of preparation parameters on properties of metakaolin-based geopolymer activated by silica fume-sodium hydroxide alkaline blend. *J. Build. Eng.* **2022**, 104984. https://doi.org/10.1016/j.jobe.2022.104984
58. Sukontasukkul, P.; Chindaprasirt, P.; Pongsopha, P.; Phoo-Ngernkham, T.; Tangchirapat, W.; Banthia, N. Effect of fly ash/silica fume ratio and curing condition on mechanical properties of fiber-reinforced geopolymer. *J. Sustain. Cem. Based Mater.* **2020**, *9*, 218–232. https://doi.org/10.1080/21650373.2019.1709999.
59. Park, S.; Yu, J.; Oh, J.E.; Pyo, S. Effect of Silica Fume on the Volume Expansion of Metakaolin-Based Geopolymer Considering the Silicon-to-Aluminum Molar Ratio. *Int. J. Concr. Struct. Mater.* **2022**, *16*, 20. https://doi.org/10.1186/s40069-022-00510-2.
60. Albidah, A.; Alghannam, M.; Abbas, H.; Almusallam, T.; Al-Salloum, Y. Characteristics of metakaolin-based geopolymer concrete for different mix design parameters. *J. Mater. Res. Technol.* **2021**, *10*, 84–98. https://doi.org/10.1016/j.jmrt.2020.11.104.

61. Supit, S.W.M.; Olivia, M. Compressive strength and sulfate resistance of metakaolin-based geopolymer mortar with different ratio of alkaline activator. *Mater. Today Proc.* **2022**, S2214785322045333. https://doi.org/10.1016/j.matpr.2022.06.514.
62. Zhao, Y.; Wnag, H.; He, Y.; Yang, L.; Wu, H. Effect of Na+ on hydration degree of alkali activated metakaolin polymer. *Mag. Civ. Eng.* **2022**, *112*, 11208. https://doi.org/10.34910/MCE.112.8.
63. Dimas, D.; Giannopoulou, I.; Panias, D. Polymerization in sodium silicate solutions: A fundamental process in geopolymerization technology. *J. Mater. Sci.* **2009**, *44*, 3719–3730. https://doi.org/10.1007/s10853-009-3497-5.